

# Microwave Emission from the Edgeworth-Kuiper Belt and the Asteroid Belt Constrained from WMAP

Kazuhide Ichikawa<sup>a,1</sup> and Masataka Fukugita<sup>a,b,c</sup>

<sup>a</sup>*Institute for Cosmic Ray Research, University of Tokyo, Kashiwa 277-8582, Japan*

<sup>b</sup>*Institute for Advanced Study, Princeton, NJ 08540 USA*

<sup>c</sup>*Institute for the Physics and Mathematics of the Universe, University of Tokyo, Kashiwa 277-8583, Japan*

## ABSTRACT

Objects in the Edgeworth-Kuiper belt and the main asteroid belt should emit microwaves that may give rise to extra anisotropy signals in the multipole of the cosmic microwave background (CMB) experiment. Constraints are derived from the absence of positive detection of such anisotropies for  $\ell \lesssim 50$ , giving the total mass of Edgeworth-Kuiper belt objects to be smaller than  $0.2M_{\oplus}$ . This limit is consistent with the mass extrapolated from the observable population with the size of  $a \gtrsim 15$  km, assuming that the small-object population follows the power law in size  $dN/da \sim a^{-q}$  with the canonical index expected for collisional equilibrium,  $q \simeq 3.5$ , with which 23% of the mass is ascribed to objects smaller than are observationally accessible down to grains. A similar argument applied to the main asteroid belt indicates that the grain population should not increase faster than  $q \simeq 3.6$  towards smaller radii, if it follows the power law continued to observed asteroids with larger radii. It is underlined that both cases are at or only slightly above the limit that can be physically significant, implying the importance of tightening further the CMB anisotropy limit, which may be attained with the observation at higher radio frequencies.

## 1. Introduction

Whether exists a substantial population of small bodies in the Edgeworth-Kuiper belt is an interesting question to ask, whichever is the origin, either remaining from the original planetary nebula or produced from the interaction among planetesimals or asteroids. The direct search for objects in the Edgeworth-Kuiper belt (we refer to them in brevity as KBO) reaches to 30 km in diameter. It is observed that KBO with the size larger than  $a_{\text{br}} \approx 40 - 100$  km decreases towards a larger size as  $a^{-q}$  with  $q \approx 4 - 5$  (Trujillo et al. 2001; Bernstein et al. 2004; Fuentes & Holman 2008; Fraser & Kavelaars 2009) (We denote by  $a$  the effective radius). The size distribution shows a break towards smaller radii at around  $a_{\text{br}} \approx 40 - 100$  km, and then flattens to be  $q \approx 3$ . With the

---

<sup>1</sup>Present address: Department of Micro Engineering, Kyoto University, Kyoto 606-8501, Japan

occultation giving the Fresnel diffraction one may observe objects smaller than a km (Bailey 1976; Dyson 1992); for recent observational efforts, see Bianco et al. (2010). Using such a technique a small KBO is recently discovered at around the radius of 300 m (Schlichting et al. 2009), which points towards a low-mass slope  $q \approx 3.9 \pm 0.3$ . These slopes and the presence of the break are understood from the consideration that they are caused by frequent destructive collisions for smaller bodies (Kenyon & Bromley 2004; Pan & Sari 2005).

Pan & Sari (2005) further argue that the slope becomes steeper again at a smaller radius and it becomes the Dohnanyi power  $q \sim 3.5$  (Dohnanyi 1969) of collisional equilibrium, when the bodies held together matter-strength dominated at around  $a \lesssim 100$  m rather than gravitationally dominated at larger radii. This is in fact the slope preferred for submicron size dust grains to account for the extinction law in optical wavelengths (Mathis, Rumpl & Nordsieck 1977; Weingartner & Draine 2001). It is interesting to see that this power of the size distribution is consistent with micron-size grains observed by the Ulysses and Galileo satellites at the Jupiter distance (Frisch et al. 1999), while the agreement with the power of the size of interstellar dust may be merely accidental. It is an interesting question if this distribution continues to super-micron sizes (Draine 2009).

Small size grains may have fallen to the Sun by the Poynting-Robertson drag, and even smaller grains may have been swept away by solar winds. The action of the Poynting-Robertson drag implies the mm size grains as the minimum size remaining in the Edgeworth-Kuiper belt after the age of the Solar System elapsed. The direct search by the Ulysses and Galileo satellites, however, shows the presence of  $\mu\text{m}$ -size grains even in the inner heliosphere around the Jupiter distance (Frisch et al. 1999), whereas the Poynting-Robertson drag gives the typical falling age to be only  $5 \times 10^4$  yr for micron-size grains.

Small bodies may aggregate to form larger bodies or may be eroded into smaller bodies. The issue of small bodies would hint us to understand the dynamics of planet formation. A possible way to explore small bodies is to look for the infrared emission from those objects (Backman et al. 1995; Teplitz et al. 1999; Kenyon & Windhorst 2001). The difficulty with the infrared emission to explore the Edgeworth-Kuiper belt objects is that the emission is largely overcome by that from the inter-planetary dust and the asteroid belt, and the subtraction of these components is not easy.

The temperature of grains in the Edgeworth-Kuiper belt is about 40K, if we assume them to be blackbody, so that they also emit microwaves in the Rayleigh-Jeans region. Such emission might be detectable in the cosmic microwave background experiment, the precision results being already available and more to come in the near future. In fact, a constraint from radio emission from such objects was recently considered in Babich et al. (2007) for the distortion of the CMB spectrum constrained by the FIRAS (Far-InfraRed Absolute Spectrometer) of the COBE satellite (Fixsen et al. 1996).

In this paper, we consider what we can learn as to the distribution of planetesimals and grains in the Edgeworth-Kuiper Belt, and also in the main asteroid belt of the Solar System from the CMB anisotropy data of Wilkinson Microwave Anisotropy Probe (WMAP) (Bennett et al. 2003;

Hinshaw et al. 2007). WMAP has measured the microwave emission in the sky, capable of making the full-sky temperature maps in five bands: 22.8, 33.0, 40.7, 60.8 and 93.5 GHz (or correspondingly the wavelengths of 13, 9.1, 7.3, 4.9 and 3.2 mm). While this does not give spectral information, it probes at a high accuracy the angular distribution, to which objects at the Edgeworth-Kuiper belt distance (and the main asteroid belt) would contribute. We aim at deriving a constraint on the total mass of the KBO and, in addition, the objects in the main asteroid belt including small grains as a function of the assumed power index of the size distribution for small objects to grains. We consider the grain size larger than  $1\mu\text{m}$ , which is large enough so that atomic and molecular excitation is unimportant and the black body approximation may apply to heating and radiation. We bear in mind the question what observational strategies would be useful to explore deeper Edgeworth-Kuiper belt objects, and also consider if future CMB experiments could detect the emission from the Edgeworth-Kuiper Belt or the main asteroid belt.

## 2. Size distribution and thermal radiation from grains

We consider the mass distribution  $n(M)$  in the broken power law  $n(M) = KM^{-\alpha}$  with two different values of  $\alpha$  for  $M_{\min} < M < M_{\text{br}}$  and  $M_{\text{br}} < M < M_{\max}$  with a break at  $M_{\text{br}}$  for KBO, as observationally indicated. We take the density of the objects to be constant at  $\rho = 2.5 \text{ g cm}^{-3}$ . The power index  $\alpha$  is then related to that of the size distribution  $q$  in  $dN/da \sim a^{-q}$  as  $\alpha = (q + 2)/3$ , and to the slope of the brightness number count of the object  $dN/dm \sim 10^{b(m-m_0)}$  as  $b = (q - 1)/5$  if the albedo is constant.

We may take the broken power law with two breaks as expected by a theoretical argument (e.g., Pan & Sari 2005), where the second break is suggested to take place at a 100 m size. The observation for KBO shows at least one break at  $\approx 40 - 100$  km radius, which is ascribed to frequent destructive collisions effective for smaller KBO. Smaller than the break size, however, the size distribution is poorly determined; the current result varies around  $q = 2.8 \pm 0.6$  (Bernstein et al. 2004; Fuentes & Holman 2008) to  $q \approx 3.9 \pm 0.3$  (Schlichting 2009), which sandwich the ‘canonical’ power of collisional equilibrium  $q = 3.5$  ( $\alpha = 11/6$ ). In view of this present observational uncertainties we adopt for KBO a broken power law with a single break at a 100 km radius, rather than introducing the second break at a smaller radius in order not to increase the number of unconstrained parameters. (For the main asteroid belt, the size distribution below the first break is reasonably determined, and we take a two-break power law; see later.)

For a larger size, we take  $q = 4.5$ , i.e.,  $\alpha = 13/6$ , consistent with the observation. For a smaller size we leave the faint end slope as a free parameter, with the canonical collisional equilibrium value  $q = 3.5$  or  $\alpha = 11/6$  in mind. The upper cutoff of the integral is taken to be the mass of Pluto,  $M_{\max} = 0.0022M_{\oplus}$  (1080 km in radius for our density  $\rho = 2.5 \text{ g cm}^{-3}$ ). Our results are insensitive to the maximum cutoff as we take  $q = 4.5$ . We take the break radius to be 100 km, or correspondingly the mass  $M_{\text{br}} = 1 \times 10^{22} \text{ g}$ , consistently with Bernstein et al. (2004).

We take two alternative choices for the minimum mass of the integral. One corresponds to  $a_{\min} = 1$  mm and the other corresponds to  $a_{\min} = 1$   $\mu$ m. The former corresponds roughly to the mass that receives the Poynting-Robertson drag for grains to fall to the Sun in the age of the Sun  $4.7 \times 10^9$  yr at the Edgeworth-Kuiper belt distance. The other is the case where a significant amount of the grain mass is included. Grains with the size smaller than  $1 \mu$ m are likely to be removed by radiation pressure in a dynamical time. We take the total mass as a parameter:

$$M_{\text{tot}} = \int_{M_{\min}}^{M_{\max}} M n(M) dM. \quad (1)$$

We take the Edgeworth-Kuiper belt distance at  $D = 40$  AU, since the consideration of a more detailed distribution would simply leave more unconstrained parameters. This simplification is sufficient for us to consider the effect. We calculate the thermal emission from KBOs, assuming that it arises from the conversion of the solar radiation absorbed by the object into IR and microwave emission, ignoring any internal sources of energy. The equation of balance for the object with radius  $a$ , albedo  $A$  and emissivity suppression factor  $\epsilon$  at the heliocentric distance  $D$  is written

$$\frac{L_{\odot}}{4\pi D^2} \cdot \pi a^2 \cdot (1 - A) = \int_0^{\infty} \pi B_{\nu}(T) \epsilon(\nu, a) d\nu \cdot 4\pi a^2, \quad (2)$$

where  $B_{\nu}(T)$  stands for the flux of the black body radiation of frequency  $\nu$  at temperature  $T$ , and  $\epsilon$  is the suppression factor when the wavelength of radiation is larger than the size of the object,

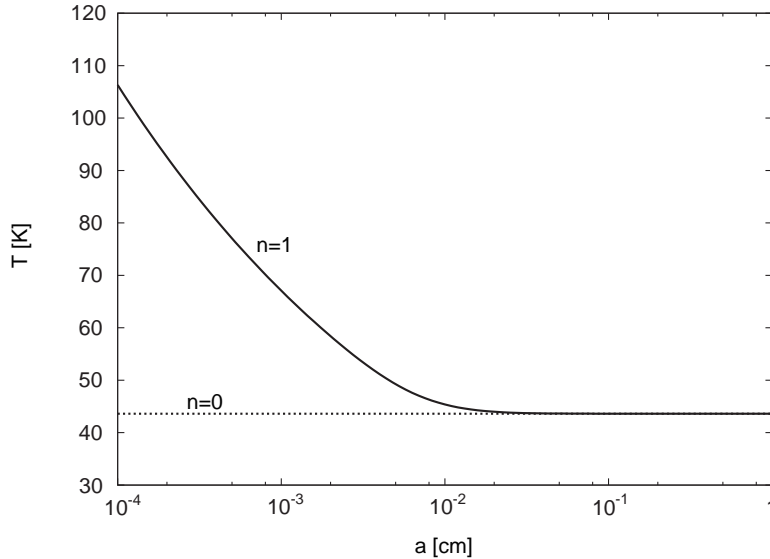


Fig. 1.— The temperature of grains at the Edgeworth-Kuiper belt distance as a function of their radius.  $n = 1$  is assumed for the power of the suppression factor in Eq. (3). We assume  $A = 0.04$  and  $D = 40$  AU.

which is assumed to be

$$\epsilon(\nu, a) = \begin{cases} 1 & \text{if } a > \lambda, \\ (a/\lambda)^n & \text{if } a < \lambda, \end{cases} \quad (3)$$

where  $\lambda$  is the wavelength.

We set  $n = 1$  as in the formal factor in Mie scattering in the following; see e.g., Spitzer (1978); Backman et al. (1995). This gives the temperature of objects at the Edgeworth-Kuiper belt distance as in Fig. 1, showing that for emission in WMAP frequencies this suppression causes some effects only for  $a < 50\mu\text{m}$ , the emission from which is unimportant for the parameters that concern us, and hence the results hardly depend on the suppression factor assumed for a wide variety of its choice. We take  $A = 0.04$ . For large size grains  $T_{\text{KBO}} = 43.7\text{ K}$ . The size of grains we consider is large enough, so that shot noise heating by a single photon is unimportant, and hence we do not treat atomic emission as was considered in detail in Weingartner & Draine (2001).

### 3. Contribution to CMB anisotropies

Let us first consider the contribution of the KBO to spectral data averaged over the sky, such as those obtained by COBE/FIRAS. This has already been done in Babich et al. (2007). We consider the two cases for  $a_{\text{min}} = 1\text{ mm}$ , as assumed in Babich et al., and for  $a_{\text{min}} = 1\mu\text{m}$ .

The KBO emission would modify the CMB spectrum averaged over the sky  $4\pi D^2 B_\nu(T_{\text{CMB}})$  as  $(4\pi D^2 - A_{\text{tot}})B_\nu(T_{\text{CMB}}) + A_{\text{tot}}B_\nu(T_{\text{KBO}})$ , where the effect is taken into account that KBOs block CMB photons over the area  $A_{\text{tot}}$  that is covered by KBOs,

$$A_{\text{tot}} = \int_{a_{\text{min}}}^{a_{\text{max}}} \pi a^2 n(a) da \quad (4)$$

The spectral distortion is written

$$\Delta B_\nu = \frac{1}{4\pi D^2} \left\{ \int_{a_{\text{min}}}^{a_{\text{max}}} \pi a^2 n(a) B_\nu(T(a)) \epsilon(\nu, a) da - A_{\text{tot}} B_\nu(T_{\text{CMB}}) \right\}. \quad (5)$$

Following Fixsen et al. (1996), we calculate  $\chi^2$  by minimizing over the shift in the CMB temperature  $\Delta T$  and the normalization factor  $G_0$  of the Galactic emission contamination template prepared by Fixsen et al. To constrain the KBO contribution, we allow  $\Delta T$  and  $G_0$  as free parameters to compute  $\chi^2 = (\Delta B_\nu + \Delta T \frac{\partial B_\nu}{\partial T} + G_0 g(\nu))^2 / \sigma_\nu^2$ , where  $g(\nu)$  is the modeled Galaxy emission spectrum: see Fixsen et al. (1996) for details. We show the limit at the 95% C.L. ( $\Delta\chi^2 = 5.99$ ) in Fig. 2. The two curves, labelled with FIRAS, shown with dashed correspond to  $a_{\text{min}} = 1\mu\text{m}$  (thick curve) and  $1\text{mm}$  (thin curve). The constraint with  $a_{\text{min}} = 1\text{mm}$ , of course, agrees with that of Babich et al. (2007), when the parameters used here are converted to theirs. The extension of the minimum cutoff radius from  $1\text{mm}$  to  $1\mu\text{m}$  modifies the result only little, no more than by a factor of 2 in mass units, unless  $\alpha$  is close to 2.

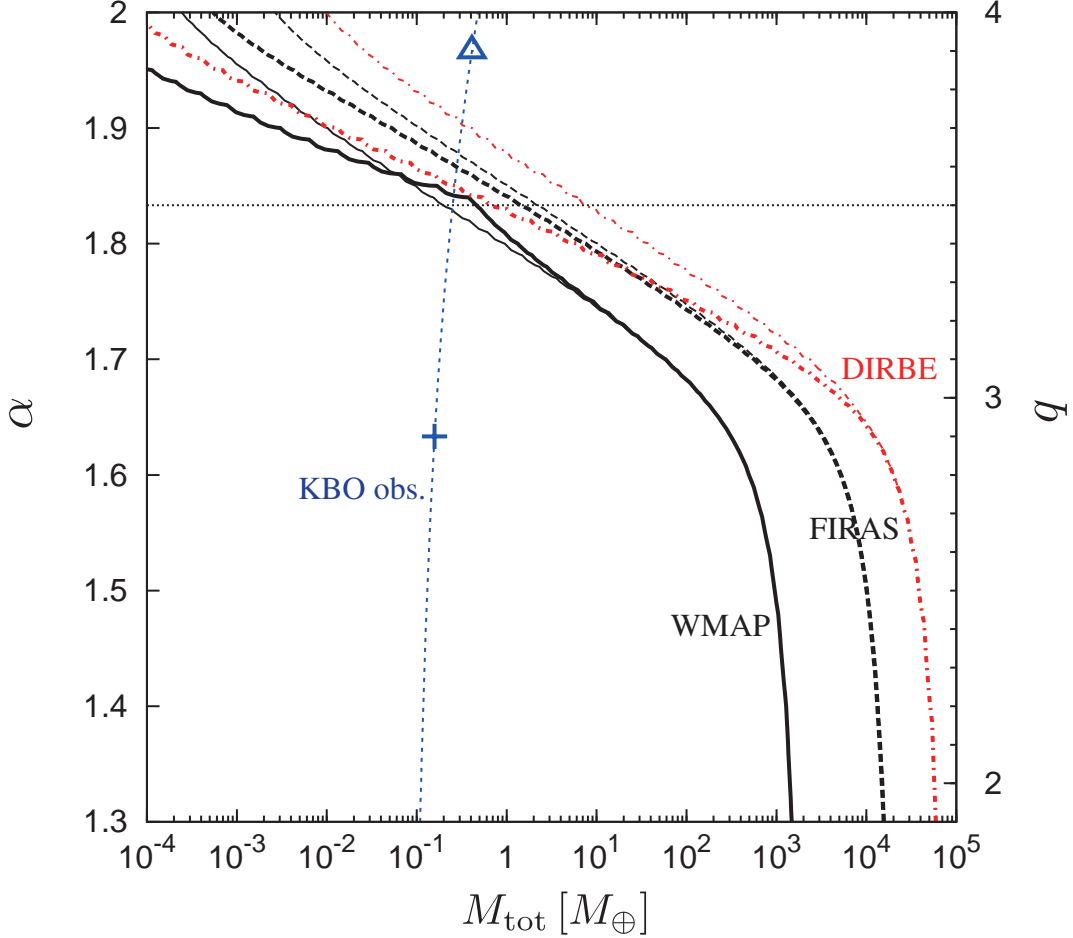


Fig. 2.— Limits on the total mass in the Edgeworth Kuiper belt as a function of the small-mass slope  $\alpha$  of the mass function at the 95% C.L. CMB anisotropy constraints from WMAP are shown with solid curves and spectral constraints from COBE/FIRAS are shown with dashed curves. The allowed regions are above the curves. Thinner lines are for  $a_{\min} = 1$  mm and thicker lines for  $a_{\min} = 1 \mu\text{m}$ . Limits from the FIR brightness of COBE/DIRBE observations are added with dash-dotted curves. The nearly vertical dotted line is the total mass of the objects in the Edgeworth-Kuiper belt extrapolated from the direct observation of larger size objects with the assumed power index of  $\alpha$ , the plus symbol being the power index estimated from the observation of objects smaller than the break radius,  $a \approx 100$  km (Bernstein et al. 2004). The triangle on the curve indicates the central value of the power index inferred from the object found in the occultation observation (Schlichting et al. 2009). The horizontal dotted line refers to the canonical power of collisional equilibrium  $q = 3.5$  of the size distribution.

We now turn to the calculation of the CMB anisotropy. We evaluate

$$\Delta B_\nu(\mathbf{n}) = \frac{f(\mathbf{n})}{D^2} \left\{ \int_{a_{\min}}^{a_{\max}} \pi a^2 n(a) B_\nu(T(a)) \epsilon(\nu, a) da - A_{\text{tot}} B_\nu(T_{\text{CMB}}) \right\}, \quad (6)$$

where  $f(\mathbf{n})$  is the spatial distribution of KBOs in the direction of  $\mathbf{n}$ , normalized to yield unity when integrated over  $\mathbf{n}$ :  $f(\mathbf{n}) A_{\text{tot}} d\Omega$  gives the area covered by KBOs at the direction  $\mathbf{n}$ . We then convert the KBO contribution to brightness  $\Delta B_\nu(\mathbf{n})$  to the temperature variation  $\Delta T(\mathbf{n})$  using the black body radiation formula. We then write it in the form  $\Delta T(\mathbf{n}) = c_\nu f(\mathbf{n})$ . Writing the KBO distribution in terms of the spherical harmonics,  $f(\mathbf{n}) = \sum_{\ell, m} f_{\ell m} Y_{\ell m}(\mathbf{n})$ , we represent the coefficient of the harmonic decomposition of  $\Delta T(\mathbf{n})$  as  $a_{\ell m}^{\text{KBO}} = c_\nu f_{\ell m}$ .

Following Brown (2001) we take the spatial distribution of KBOs to be double Gaussian around the ecliptic plane

$$f(\mathbf{n}) \propto \sum_i A_i \exp \left\{ -\frac{(\theta - \theta_{\text{ecl}})^2}{2\sigma_{\text{KBO},i}^2} \right\}, \quad (7)$$

where  $\theta_{\text{ecl}} \sim 60^\circ$  is the inclination angle between the ecliptic plane and the Galactic plane. We take the widths of the distribution of classical KBO's,  $\sigma_{\text{KBO},1} = 2^\circ.2$  and  $\sigma_{\text{KBO},2} = 17^\circ$  with the ratio of the coefficients  $A_1 : A_2 = 0.65 : 0.35$  from the observed latitudinal distribution.

The multipole coefficient of the CMB power spectrum is modified by emission from KBOs as

$$\begin{aligned} C_\ell &= \frac{1}{2\ell+1} \sum_{m=-\ell}^{\ell} |a_{\ell m}^{\text{CMB}} + a_{\ell m}^{\text{KBO}}|^2, \\ &= C_\ell^{\text{CMB}} + C_\ell^{\text{KBO}} + \frac{1}{2\ell+1} \sum_{m=-\ell}^{\ell} 2\text{Re } a_{\ell m}^{\text{CMB}} a_{\ell m}^{*\text{KBO}}. \end{aligned} \quad (8)$$

We show an example of harmonics  $C_\ell$  at  $\nu = 93.5$  GHz, the highest frequency band of WMAP. The contribution expected from KBO emission is shown for the parameters,  $M_{\text{tot}} = 1M_\oplus$  and  $\alpha = 1.83$  in Fig. 3, which represent a case marginally allowed by COBE/FIRAS, but will be rejected by the WMAP observation as shown in what follows (see Fig. 2). The KBO contribution shows the maximal power at around,  $\ell \approx 20 - 30$ . The emission from the KBO for  $\ell \lesssim 100$ , with the choice of the trial parameters taken here, is only slightly larger than the cosmic variance. The cross correlation signal,  $C_\ell^{\text{cross}}$ , given by the last term in Eq.(8), is much smaller.

With the lack of any signals indicating the contribution of KBO emission we may set  $a_{\ell m}^{\text{CMB}}$  to the observed value. The error bars attached to the CMB data are the cosmic variance

$$\frac{\sigma_\ell}{C_\ell^{\text{CMB}}} = \sqrt{\frac{2}{2\ell+1}}. \quad (9)$$

The accuracy of the WMAP observation for  $\ell \lesssim 100$  that concerns us here already reaches the cosmic variance.

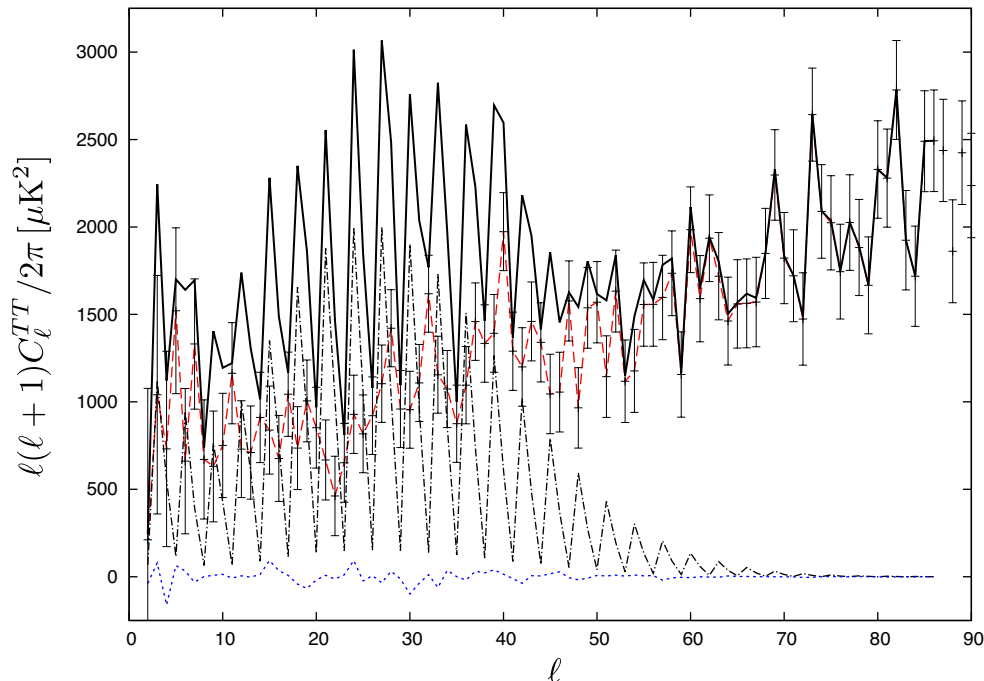


Fig. 3.— Example of multipoles of temperature anisotropy. The red dashed line shows  $C_\ell^{CMB}$ , the dot-dashed line shows  $C_\ell^{KBO}$  and blue dotted line indicates the cross term  $C_\ell^{cross}$ , where the parameters for KBO are taken to be  $M_{tot} = 1M_\oplus$  and  $\alpha = 1.83$ , the parameters allowed by a COBE/FIRAS spectral analysis but is forbidden by WMAP anisotropies. The total multipole is shown by the solid line  $C_\ell$ . The error bars depict the cosmic variance.

We may derive the constraint from the CMB data, by requiring that the KBO contributions and the interference term between CMB and KBO,  $C_\ell^{KBO} + C_\ell^{cross}$  be smaller than the cosmic variance. The result does not change if we replace the cosmic variance with the observed WMAP data. We calculate  $\chi^2$  as

$$\chi^2 = \sum_{\nu} \sum_{\ell} \frac{(C_\ell^{KBO} + C_\ell^{cross})^2}{\sigma_\ell^2}, \quad (10)$$

where the summation  $\nu$  is over the data in the three highest frequency bands  $\nu = 93.5$  GHz, 60.8 GHz and 40.7 GHz of the WMAP. The result is shown with solid curves in Fig. 2 above for both  $a_{min} = 1\mu m$  (thick curve) and 1 mm (thin curve). The limit is derived basically from the highest frequency data, and the inclusion of lower frequency data modifies little the result. The curve for  $a_{min} = 1\mu m$  generally appears lower in the figure (i.e., the limit being tighter) than that for  $a_{min} = 1mm$ , but the two curves are reversed at a specific  $\alpha$ , where the integrand of Eq. (6) vanishes for some value of  $\alpha$  owing to the presence of the suppression factor:  $\Delta B_\nu$  in Eq. (5) can be negative at some value of  $\nu$  for small grains ( $a \ll 1mm$ ), which in turn allows extra emission from larger objects given the total emission as the constraint. For the canonical power index  $q = 3.5$ ,



the limit of the KBO with  $a_{\min} = 1\text{mm}$  is  $0.2 M_{\oplus}$ , of which 23 % of the mass arises from the objects below the limit of the observed KBO  $a \approx 15\text{ km}$ . The KBO radiation arises dominantly from objects with  $a \leq 15\text{ km}$  if  $q \geq 3.2$ . The anisotropy data give a limit stronger than the spectral distortion by a factor of  $\approx 5$  in the total mass.

In the same figure, we also display the limit from the FIR emission using the COBE/DIRBE data which are already discussed by Teplitz et al. (1999). We take the observed FIR data (Hauser et al. 1998) to derive the bound. The limit on the KBO emission should actually be tighter, if the FIR emission from interplanetary dust and the asteroid belt which give rise to the FIR signal could properly be subtracted. The reliable subtraction to give a small component, such as cosmic infrared background, however, is notoriously difficult. So, we take here the observed brightness without subtraction. If we would take the modest subtraction, for example, of Hauser et al. (1998) and take their ‘cosmological infrared background’, which amounts to half the observed brightness, the limit comes somewhat close to the curve that is obtained from WMAP.

The additional curve in the figure (nearly vertical dotted curve) is the extrapolation of the KBO detected by Bernstein et al. (2004) to include smaller objects assuming that the population persists to grain size objects and the power law with the free-parameter index specified in the ordinate for objects smaller than the break radius. The plus symbol on the curve indicates the power index they inferred for the objects immediately below the break radius, and the triangle the index inferred from one object found in the occultation observation (Schlichting et al. 2009). The nearly vertical nature of this curve means that small objects contributes to the total mass only by a small amount. It is interesting to note that the anisotropy limit (with  $a_{\min} = 1\text{mm}$ ) crosses the extrapolation of the observed objects just at the canonical slope  $\alpha = 1.83$  ( $q = 3.5$ ). This means that the limit on mass from CMB anisotropy experiment is just consistent with the mass estimate from the observation of KBOs extrapolated to small size objects for the canonical power index, although the total mass of observable KBOs is not accurately determined. If the small population of KBO has the size distribution of the canonical power, as we may see some indication around the Jupiter distance for the ‘asteroid’ grains from the Ulysses and Galileo satellite (Frisch et al. 1999), emission from KBO is marginally detectable with CMB anisotropies. The anisotropy data barely have a power to detect such a contribution, if not detected with the present data yet.

Finally let us ask what information can be obtained from CMB anisotropy as to grains in the main asteroid belt. The temperature of asteroids  $\approx 170\text{K}$  may appear significantly higher than that relevant to CMB, but these grains should also emit microwaves in the tail of the Rayleigh-Jeans region. Following the observation (Ivezić et al. 2001) we take the mass distribution of asteroids that has the power index  $\alpha = 2.0$  ( $q = 4$ ) for  $2.5 < a < 20\text{ km}$  and  $\alpha = 1.43$  ( $q = 2.3$ ) for  $0.2 < a < 2.5\text{ km}$  with the break radius  $a_{\text{br}} = 2.5\text{ km}$ . We extend the distribution to the Ceres radius (450km) for large size asteroids in our integration. On the other hand we extend the distribution to small grains by introducing the possible second break at the limiting radius of the observation at  $0.2\text{ km}$ , leaving the power index  $\alpha$  as a parameter for smaller bodies beyond the second break radius. The experiment of Ulysses and Galileo indicates that micrometre-size grains follow the distribution with

$a \approx 1.83$  ( $q \approx 3.5$ ), although no information is available as to grains larger than a few micrometre size, nor we know if this grain population is related to the small asteroid population.

We carry out a similar calculation for the main asteroid belt at the average of 2.6 AU, as did for the microwave emission from KBO, in order to glance the possible contribution from the main belt. We assume the Gaussian distribution with  $\sigma = 10^\circ$  for the main asteroid belt, which is broadly consistent with the observation (Ryan et al. 2009). We give limits in Figure 4, both from the absence of the spectral distortion constrained by COBE/FIRAS (Fixsen et al. 1996) and of excess anisotropies by WMAP (Hinshaw et al. 2007), the latter leading to the limit stronger than the former, again by a factor of 5 in mass. The limit thus derived may be compared with the estimate of the total mass of asteroids,  $\approx 0.0005M_\oplus$  for the observable population (Bottke et al. 2002; Ryan et al. 2009). It is interesting to note that the limit on the mass  $\lesssim 0.001M_\oplus$  with the canonical power  $q \approx 3.5$  appears close to what is observed for the asteroid belt. We remark that the limit with  $M_{\min} = 1\text{mm}$  (thin curve) appears below the curve with  $M_{\min} = 1\mu\text{m}$  (thick curve) in the small total mass end in the figure due to the cancellation of the emissivity close to  $\alpha \approx 1.93$  arising from the suppression factor, as we noted above for the case with KBO.

The nearly vertical dotted curve is the extrapolation of the observed component of asteroids. This indicates that grains contribute little to the total mass; it is basically determined by the observed asteroids ( $a > 0.2$  km). The contribution to the total mass from objects smaller than are observable, for instance, is only by 1% if  $q = 3.5$ . The plus symbol on the curve is the power index derived from the observation of asteroids smaller than the first break radius down to the observational limit. The canonical collisional equilibrium power is indicated by the horizontal dotted line.

The curve of CMB limit shows that  $\alpha$  should be smaller than 1.87 ( $q < 3.6$ ) for the assumed power-law extension of the asteroid population to smaller sizes, in order to be consistent with the absence of the extra CMB anisotropy. The significance of this figure is that the WMAP limit crosses with the extrapolation from the observed asteroid at  $\alpha$  close to the value that indicates the canonical collisional equilibrium power or that is inferred from the Ulysses and Galileo satellite observation. That is, the limit is just consistent with the possibility that the grain population detected by those satellites is the small-size tail of the observed asteroid population. If the grain population would follow the power law and continue to what was found by the Ulysses and Galileo satellite,  $q \approx 3.5$  (Frisch et al. 1999), the contribution of the microwave emission is marginally detectable, if the anisotropy limit could be made tighter by a factor of 2 – 3. See discussion in the next section.

#### 4. Discussion and conclusion

We have shown that the microwave radiation from small bodies in the Solar System would give excess anisotropy in the microwave sky, and contribute to the multipole coefficient at low- $\ell$  in excess

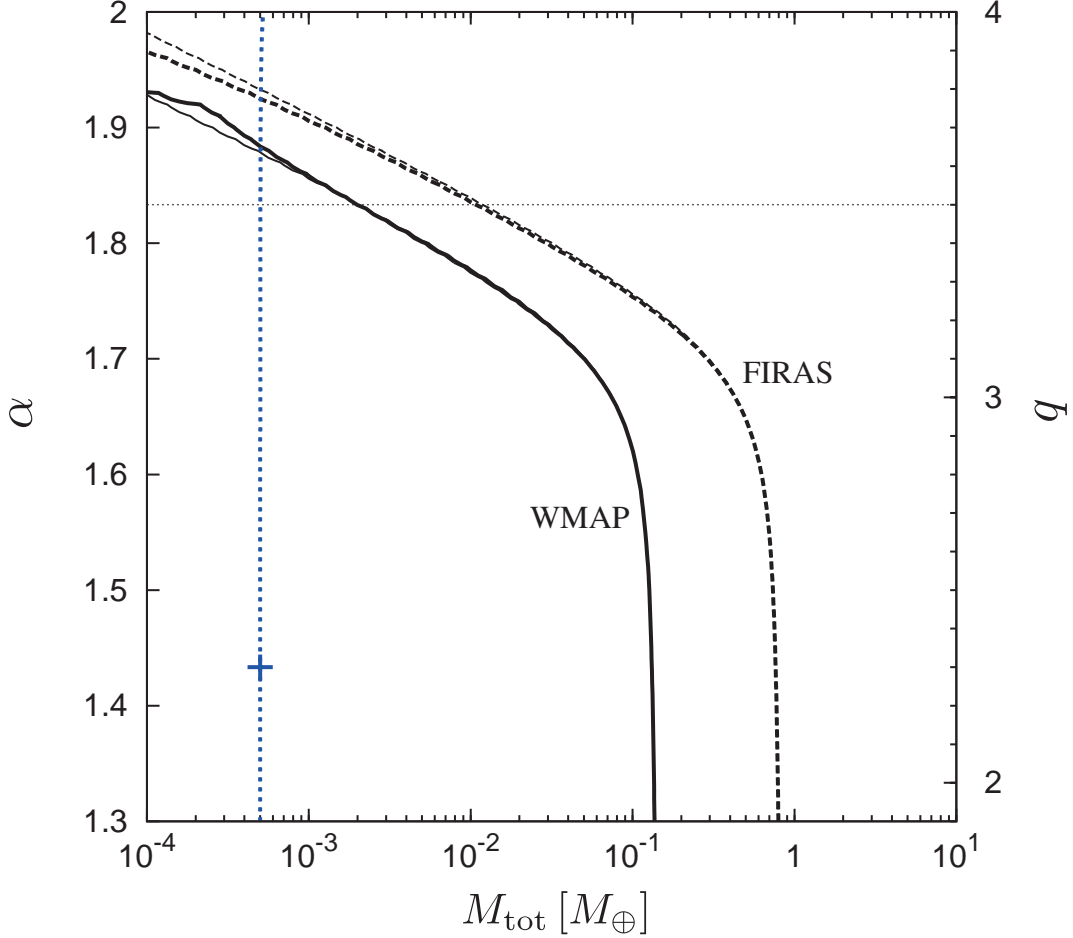


Fig. 4.— Limits on the mass in the asteroid belt as a function of the small-mass slope  $\alpha$  of the mass function at the 95% C.L. CMB anisotropy constraints from WMAP and spectral constraints from COBE/FIRAS are shown with solid and dashed curves, respectively. The allowed regions are above the curves. Thinner lines are for  $a_{\min} = 1$  mm and thicker lines for  $a_{\min} = 1$   $\mu$ m. The nearly vertical dotted line is the total mass of the asteroids extrapolated from the direct observation with the power index of  $\alpha$ . The plus symbol is the power index estimated from the observation of asteroid just below the (first) break radius. The horizontal dotted line refers to the canonical power of collisional equilibrium  $q = 3.5$  of the size distribution.

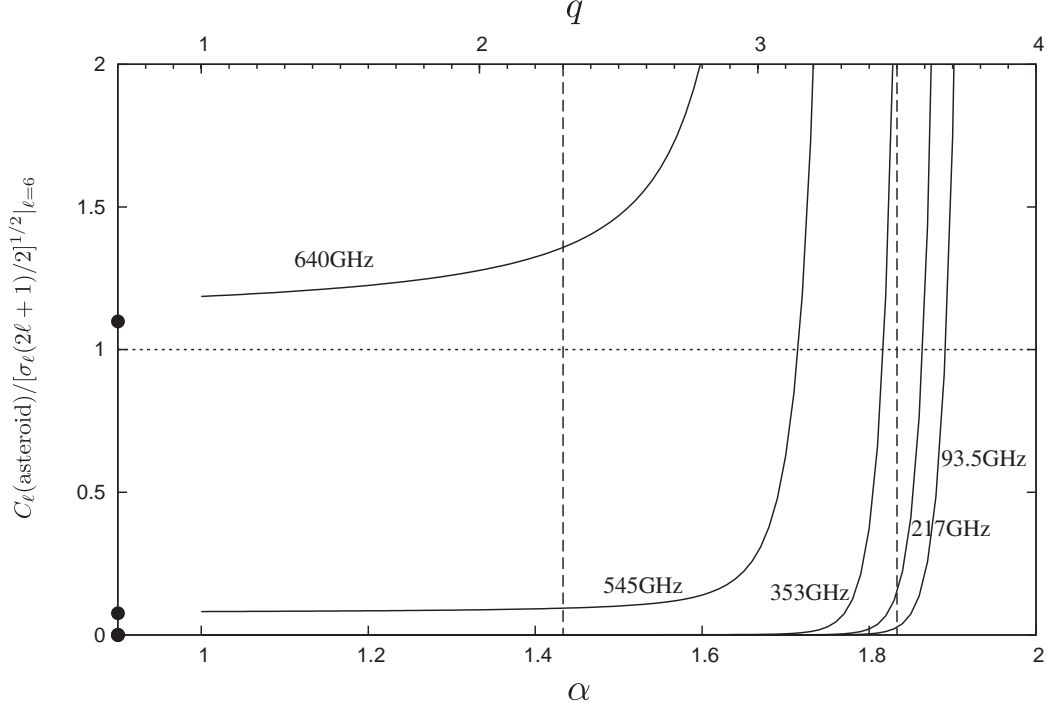


Fig. 5.— Expected contribution of the asteroid signal to the CMB multipole compared with the cosmic variance  $C_\ell(\text{asteroid})/[\sigma_\ell(2\ell + 1)/2]^{1/2}$  at the multipole,  $\ell = 6$ , as a function of the power index of the small-size objects  $\alpha$  for several choices of frequency  $\nu$ . The symbols on the left ordinate indicate the expected asteroid signal from the observed population ( $a > 0.2\text{km}$ ) of asteroid belt alone. The dotted line is the canonical power of collisional equilibrium  $q = 3.5$  (or the power index of grains detected in the Ulysses Galileo mission) and the power of smaller observed asteroids.

of the proper CMB anisotropy. The current CMB anisotropy experiment, which reaches the cosmic variance for small  $\ell$ , already gives an upper limit on the Edgeworth-Kuiper belt objects stronger than others available to date. If  $q = 3.5$ , the canonical power index for collisional equilibrium, the limit is  $< 0.2 M_\oplus$ , where about 80% of the mass arises from objects with  $a > 15\text{ km}$  that could be accessible in the optical observation available to date. The application to the microwave emission from the asteroid belt shows that the grain population should not increase to smaller radii as fast as  $q > 3.5$ . The limit is close to the canonical power index. If there is a population that interpolates asteroids and grains found by Ulysses-Galileo satellite, it would cause a signal marginally detectable when the anisotropy limit would be improved, say, by a factor of 2. In summary, we would underline that the current limit set from CMB anisotropy is just above what could be significant to understand the world of small asteroids and grains for both Edgeworth-Kuiper belt and main asteroid belt. Tightening of the anisotropy limit by a factor of 2 or 3 would bring us a significant new insight.

The current limit from microwave emission from asteroids is derived taking the cosmic variance,

which was already reached by WMAP for  $\ell$  that concerns us. This means that we are not readily able to strengthen the limit by improving the experimental accuracy. We may think of two ways, however, to improve the limit or possibly detect the signal. One is to work with higher frequency (e.g., in the Planck satellite, which observes, e.g., at 217, 353, 545 and 857 GHz) where the relative importance of grain emission increases with  $\nu^2$ , as anticipated in the Rayleigh-Jeans region, while the CMB is in the Wien region beyond 150 GHz. Repeating similar calculations, we have confirmed that the CMB anisotropy limit goes beyond what is expected from the extrapolation of the KBO observations with the canonical power of  $q = 3.5$  if the 353 GHz observation with the Planck satellite (Lamarre et al. 2010) would not see any signals beyond the cosmic variance.

Similarly, the CMB anisotropy limit on the asteroids in the main belt also comes beyond the crossing point of the extrapolation of observed asteroid with the  $q = 3.5$  power if 353 GHz is used. Figure 5 shows the asteroid signal compared with the cosmic variance,  $C_\ell(\text{asteroid})/[\sigma_\ell(2\ell+1)/2]^{1/2}$ , at an optimal multipole for the main asteroid belt,  $\ell = 6$ , as a function of the power index of the small-size objects  $\alpha$  for several choices of frequency  $\nu$  (we took some of them as values used by the Planck mission). The symbols on the left ordinate are the expected CMB signals from the observed population of asteroids alone. The curves include the contributions from small objects extrapolated with a power law with the index  $\alpha$  down to 1 mm size. This shows that the signal appears beyond the cosmic variance for the observation with  $\nu \gtrsim 350$  GHz if small size objects obey the power law with the canonical power: for  $\nu \gtrsim 640$  GHz the emission from the observed population of asteroids alone will exceed the cosmic variance at the  $\ell = 6$  multipole. This brief analysis would warrant more realistic modelling of the microwave emission from the main asteroid belt, including its three dimensional structure, and a more detailed analysis.

The other way to tighten the limit may be to use a templet filter that matches the spatial distribution of objects in the Edgeworth-Kuiper belt or the asteroid belt to enhance their signals. A possibility is not yet excluded for a detection of microwave emission from small bodies in anisotropy measurements.

We would like to thank Bruce Draine for useful comments.

## REFERENCES

- Babich, D., Blake, C. H., & Steinhardt, C. L. 2007, ApJ, 669, 1406
- Backman, D. E., Dasgupta, A., & Stencel, R. E. 1995, ApJ, 450, L35
- Bailey, M. E. 1976, Nature, 259, 290
- Bennett, C. L., et al. 2003, ApJS, 148, 1
- Bernstein, G. M., Trilling, D. E., Allen, R. L., Brown, M. E., Holman, M., & Malhotra, R. 2004, AJ, 128, 1364

- Bianco, F. B., et al. 2010, *AJ*, 139, 1499
- Bottke, W. F., Jr., Cellino, A., Paolicchi, P., & Binzel, R. P. 2002, *Asteroids III* (Tucson: University of Arizona Press), p. 3
- Brown, M. E. 2001, *AJ*, 121, 2804
- Dohnanyi, J. S. 1969, *J. Geophys. Res.*, 74, 2531
- Draine, B. T. 2009, *Space Sci. Rev.*, 143, 333
- Dyson, F. J. 1992, *QJRAS*, 33, 45
- Fixsen, D. J., Cheng, E. S., Gales, J. M., Mather, J. C., Shafer, R. A., & Wright, E. L. 1996, *ApJ*, 473, 576
- Fraser, W. C., & Kavelaars, J. J. 2009, *AJ*, 137, 72
- Frisch, P. C., et al. 1999, *ApJ*, 525, 492
- Fuentes, C. I., & Holman, M. J. 2008, *AJ*, 136, 83
- Greenberg, J. M. 1978, *Cosmic Dust*, 187
- Hauser, M. G., et al. 1998, *ApJ*, 508, 25
- Hinshaw, G., et al. 2007, *ApJS*, 170, 288
- Ivezić, Ž., et al. 2001, *AJ*, 122, 2749
- Kenyon, S. J., & Bromley, B. C. 2004, *AJ*, 128, 1916
- Kenyon, S. J., & Windhorst, R. A. 2001, *ApJ*, 547, L69
- Lamarre, J.-M., et al. 2010, *A&A*, 520, A9
- Mathis, J. S., Rumpl, W., & Nordsieck, K. H. 1977, *ApJ*, 217, 425
- Pan, M., & Sari, R. 2005, *Icarus*, 173, 342
- Ryan, E. L., et al. 2009, *AJ*, 137, 5134
- Schlichting, H. E., Ofek, E. O., Wenz, M., Sari, R., Gal-Yam, A., Livio, M., Nelan, E., & Zucker, S. 2009, *Nature*, 462, 895
- Spitzer, L. 1978, *Physical Processes in the Interstellar Medium*, New York: Wiley & Sons, 1978
- Teplitz, V. L., Stern, S. A., Anderson, J. D., Rosenbaum, D., Scalise, R. J., & Wentzler, P. 1999, *ApJ*, 516, 425

Trujillo, C. A., Jewitt, D. C., & Luu, J. X. 2001, *AJ*, 122, 457

Weingartner, J. C., & Draine, B. T. 2001, *ApJS*, 134, 263